Mineralogical and chemical characterization of supergene copper-bearing minerals: examples from Chile and Burkina Faso

Zia Steven Kahou, Stéphanie Duchêne, Stéphanie Brichau, Eduardo Campos, Guillaume Estrade, Marc Poujol, Janogithan Kathirgamar, Hugo Testa, Mathieu Leisen, Sandrine Choy, et al.

Journal Pre-proofs

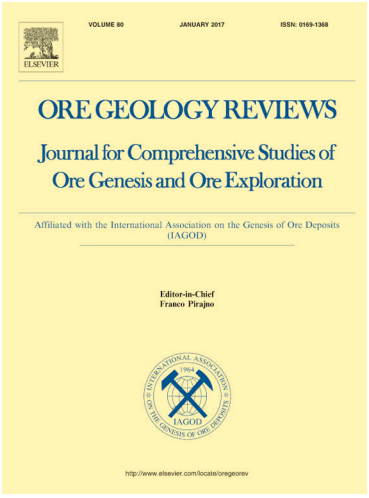

Mineralogical and chemical characterization of supergene copper-bearing minerals: examples from Chile and Burkina Faso

Zia Steven Kahou, Stéphanie Duchêne, Stéphanie Brichau, Eduardo Campos, Guillaume Estrade, Marc Poujol, Janogithan Kathirgamar, Hugo Testa, Mathieu Leisen, Sandrine Choy, Philippe de Parseval, Rodrigo Riquelme, Sébastien Carretier

PII: S0169-1368(21)00103-7
DOI: https://doi.org/10.1016/j.oregeorev.2021.104078
Reference: OREGEO 104078

To appear in: *Ore Geology Reviews*

Received Date: 7 July 2020
Revised Date: 7 February 2021
Accepted Date: 20 February 2021

Please cite this article as: Z.S. Kahou, S. Duchêne, S. Brichau, E. Campos, G. Estrade, M. Poujol, J. Kathirgamar, H. Testa, M. Leisen, S. Choy, P. de Parseval, R. Riquelme, S. Carretier, Mineralogical and chemical characterization of supergene copper-bearing minerals: examples from Chile and Burkina Faso, *Ore Geology Reviews* (2021), doi: https://doi.org/10.1016/j.oregeorev.2021.104078

Mineralogical and chemical characterization of supergene copper-bearing minerals: examples from Chile and Burkina Faso

Zia Steven Kahou[1], Stéphanie Duchêne[1], Stéphanie Brichau[1], Eduardo Campos[2], Guillaume Estrade[1], Marc Poujol[3], Janogithan Kathirgamar[1], Hugo Testa[1], Mathieu Leisen[1], Sandrine Choy[1], Philippe de Parseval[1], Rodrigo Riquelme[3], Sébastien Carretier[1]*

1. Géosciences Environnement Toulouse (GET), Université de Toulouse, UPS, CNRS, IRD, CNES, 14 avenue E. Belin, 31400, Toulouse, France
2. Departamento de Ciencias Geológicas, Universidad Católica del Norte, Avenida Angamos 0610, Antofagasta, Chile
3. Univ Rennes, CNRS, Géosciences Rennes – UMR 6118, F-35000 Rennes, France

*Corresponding author: steven.kahou@get.omp.eu - (+33) 0782808145

Abstract

Using optical microscopy, SEM, EPMA and LA-ICP-MS, we analyzed and characterized the textural features of Cenozoic supergene Cu-bearing minerals from three exotic and two *in situ* supergene copper mineralization from the Atacama Desert in northern Chile. In addition, we analyzed their major and rare earth elements compositions. We then compared these data to those obtained from the *in situ* supergene copper mineralization from the Gaoua Cu-Au porphyry district, emplaced during the Cenozoic in a different geodynamic setting in the West African craton. In both the *in situ* and exotic supergene copper mineralization, chrysocolla is the dominant supergene copper-bearing mineral, followed by pseudomalachite with minor amount of copper wad. Chrysocolla and pseudomalachite show distinct textural features. Chrysocolla appears either as black Mn-rich clasts or light-blue to green masses, filling the fractures and coating the non-mineralized clasts. Pseudomalachite occurs as green color bands or thin coatings filling empty spaces. All the deposits share some common features with regard to their major element and REE compositions, i.e. i) same range of chemical compositions suggesting similar conditions of formation and ii) strong Ce anomaly indicative of oxidant conditions during the crystallization of these supergene copper minerals. Our results reflect similar conditions for the formation of both supergene copper minerals in all the mining districts and lead us to propose that

both areas (i.e. the Atacama Desert and southwestern Burkina Faso) underwent similar geological and climatic conditions in order to form and preserve supergene copper mineralization, i.e. exhumation of the porphyry copper deposit and weathering of the primary copper sulfides, downward and laterally moving of copper-bearing solutions to form *in situ* and exotic SCM and finally, arid to hyperarid climate to prevent mechanical abrasion and leaching of the newly formed supergene copper mineralization.

Keywords: *in situ* and exotic supergene copper mineralization; Atacama Desert; Gaoua Cu-Au district; black chrysocolla; chrysocolla; pseudomalachite

1. Introduction

Supergene copper mineralization (SCM) is produced by the interaction between sulfides and supergene processes and was originally defined by Ransome (1912) as *sulfide oxidation and leaching of ore deposits in the weathering environment, and any attendant secondary sulfide enrichment*. In order to form supergene copper mineralization, specific tectonics, climate and geomorphologic conditions are required. Tectonics controls the uplift needed to lower the groundwater table and raise the deep-seated ore deposits towards more oxidizing environments were the oxidation and leaching of sulfides may occur. On the other hand, climate controls water availability, and therefore the leaching of sulfides and remobilization of copper-bearing solutions in the supergene environment towards the locus where supergene copper-bearing minerals precipitate. Then, favorable geomorphologic conditions prevent major erosion and removal of the supergene mineralized bodies (Hartley and Rice, 2005; Sillitoe, 2005). Two types of SCM have been recognized: 1) *in situ* deposits, which are produced by nearly vertical descending Cu-bearing aqueous solutions and precipitation of SCM within or near the leached cap (Sillitoe, 2005); and 2) exotic deposits, which are originated by lateral migration of Cu-bearing solutions from the parental deposit, without direct link with the original source of metal (Fig. 1, Münchmeyer, 1996; Sillitoe, 2005). In order to better understand the genesis of *in situ* and exotic SCM deposits and the parameters controlling their formation, mineralogical and geochemical characterization are required. To the best of our knowledge, apart from the work of Chavez (2000) who described in detail the zoning and distribution of copper oxide minerals in SCM in general, all the previous studies have been focused on the description of single SCM deposits and the characterization of the secondary K-bearing minerals that are genetically linked to the precipitation of copper-bearing minerals (Alpers and Brimhall, 1988; Bouzari and Clark, 2002; Cuadra and Rojas, 2001; Kahou et al., 2020; Marsh et al., 1997; Mote et al., 2001a). Furthermore, most of these studies have been carried out in the Atacama Desert and southwest USA. However, SCM can be observed all around the world (Fig. 2A) and were therefore formed under various climatic and tectonic conditions (e.g. Atacama Desert, SW of U.S.A, northern Mexico, Mongolia, Papua New Guinea, Philippines, western and central Africa, etc…). Here

we present a comparison of SCM deposits in two contrasting geological and climatic settings, the Atacama Desert and the southwestern region of Burkina Faso.

For decades, the Atacama Desert represents an ideal location to study SCM because of the presence of world-class examples of both *in situ* (Chuquicamata, Salvador, Cerro Colorado, Zaldivar-Escondida Norte, etc.) and exotic (Mina Sur, Damiana, Tesoro, etc.) SCM formed within an active continental margin under hyperarid climate resulting from the interaction between the uplift of the Andean mountain and the intensification of the Humboldt Current (Garreaud et al., 2010). In this area, we focused our study on Zaldivar and Gaby *in situ* SCM and Mina Sur, Damiana and El Cobre exotic SCM, all formed during the Eocene to Miocene epochs. As a contrasted example, we also studied the *in situ* SCM of Gaoua, in Burkina Faso, emplaced during the Cenozoic, and located in a passive tectonic margin under a much wetter climate (i.e. sub-humid to Sahelian climate).

In more details, we carried out an intensive mineralogical and mineral chemistry studies of the oxidized copper ores using optical microscopy and SEM to describe the textural features together with EPMA and LA-ICPMS analyses for a chemical characterization. All the acquired data were then combined in order in order to better constrain the main factors controlling the genesis of SCM. The mineralogical characterizations show that Atacama Desert and SW Burkina Faso underwent similar processes during the SCM formation and preservation despite geodynamic differences. Our new chemical study confirms and implements previous ones (Chávez, 2000; Fernández-Mort et al., 2018; Sillitoe, 2005) by pointing out that exotic SCM deposits were formed under uninterrupted oxidizing conditions while *in situ* SCM deposits show changes in the redox conditions during their formation.

2. Geological Background

The Atacama Desert is worldwide known to host some of the world's largest porphyry copper deposits, e.g. Escondida, Chuquicamata and Collahuasi. Most of these deposits are located in the Precordillera, a near N-S trending pre-Andean mountain range that extends over 800 kilometers and corresponds to a former magmatic arc formed during the Incaic orogeny (Fig. 2B; Mpodozis and Ramos, 1989; Amilibia et al., 2008; Mpodozis and Cornejo, 2012). This mountain range contains most of Chile's porphyry copper deposit and is made up of Late Paleozoic to Eocene blocks, delimited by

inverted normal and strike-slip faults (Scheuber and Reutter, 1992). In the Atacama Desert, the emplacement of hydrothermal alteration and hypogene mineralization was synchronous with the formation of the Precordillera (Sillitoe and Perelló, 2005) while supergene alteration occurred at least ~ 11 m.y. after the last hydrothermal event (Sillitoe and McKee, 1996).

The Mina Sur exotic copper deposit (Fig. 2B) is located within the Chuquicamata mining district, the second biggest Cu producer in the world. Geological, petrological and tectonic features of the Chuquicamata porphyry copper as well as the Mina Sur exotic copper deposits have been discussed in detail by previous authors (Dilles et al., 2011; Mortimer et al., 1977; Mpodozis and Cornejo, 2012; Newberg, 1967; Ossandón et al., 2001; Rivera et al., 2012; Sillitoe and Perelló, 2005) and are only briefly summarized here. In response to the uplift of the Precordillera, several forearc basins were formed during the Late Tertiary (Scheuber et al., 1994) including the Calama basin, which hosts the Mina Sur exotic copper deposit. The basement of this basin is represented by a metamorphic Paleozoic complex, extensively faulted and brecciated and by a Permian to Carboniferous Igneous complex (Ossandón et al., 2001; Rivera et al., 2012). The Calama formation and the El Loa group (Tomlinson et al., 2001), both made of continental sedimentary to volcano-sedimentary erosional gravels (May et al., 2010, 1999) lie above this basement. An ignimbrite flow deposited on top of the gravels was dated at 8.4 ± 0.4 Ma by K/Ar on biotite (Mortimer et al., 1977), which gives a minimum depositional age for these gravels. The exotic copper mineralization, which comprises copper silicates, copper phosphates, copper carbonates and copper halides is observed either filling fractures on the bedrock or the empty spaces available between the gravels.

The Damiana exotic copper deposit originates from the lateral migration of copper solutions from the Salvador porphyry copper deposit, within the El Salvador Mining District (Fig. 2B). This mining district has been well studied by Gustafson and Hunt (1975), Cornejo et al. (1997), Gustafson et al. (2001) and Mote et al. (2001b). The district is located near the Sierra Castillo fault, which represents the southern segment of the Domeyko fault system. The Domeyko fault system is a near N-S trending major zone of deformation in the Precordillera, related to the emplacement of some of the most important porphyry copper deposits in the Atacama Desert (Mpodozis and Cornejo, 2012). The bedrock of the mining district is made of a Paleocene rhyolitic dome complex, named the Cerro Indio Muerto,

which has been intruded by hypogene mineralized porphyries (Cornejo et al., 1997). The exotic copper mineralization in the Damiana deposit is filling fractures that are present in the Early Cretaceous volcanoclastic rocks *a.k.a.* the Llanta formation (Bissig and Riquelme, 2010; Rojas and Muller, 1994). This mineralization is also within the gravels (i.e. Atacama Pediplain), filling paleochannels around the Cerro Indio Muerto. Finally, ignimbrite flow and tuff, dated at 11.6 ± 0.5 Ma and 12.5 ± 0.5 Ma respectively (Sillitoe et al., 1968), cover the Atacama pediplain and yield a minimum age for the deposition of the pediment.

The El Cobre exotic deposit is linked to the Potrerillos porphyry copper deposit located approximately 30 Km to the southeast of El Salvador deposit, in the Potrerillos mining district (Fig. 2B; Bissig and Riquelme, 2009). Previous studies discussed the geology as well as the structural features of the Potrerillos porphyry copper deposit (Bissig and Riquelme, 2009; Marsh et al., 1997), indicating that this deposit is linked to the Sierra Castillo fault and is hosted by Jurassic to Cretaceous marine and volcano-sedimentary rocks. Hypogene mineralization of the Potrerillos porphyry copper deposit were emplaced during the late Eocene (~36-35 Ma; Marsh et al., 1997). At El Cobre exotic deposit, copper mineralization was deposited within the fractured and brecciated Paleocene andesitic and rhyolitic volcanic rocks (Bissig and Riquelme, 2009), which provide therefore a maximum age for their deposition.

The Zaldivar and Gaby *in situ* SCM are also located within the Precordillera of northern Chile (Fig. 2B). Zaldivar is part of the Escondida cluster, which represents the biggest copper district in the world whilst Gaby is located ~ 100 Km south of Chuquicamata and ~ 43 Km east of Spence porphyry copper deposit. The formation of both deposits is linked to the compressional and transtensional movements of the Domeyko fault system, related to the Incaic orogenic event (Mpodozis and Cornejo, 2012). Country rocks at Zaldivar is made of the La Tabla formation (Urzua, 2009), a set of Early Permian rhyolite to dacite ignimbrite and volcanic rocks. The latter are intruded by granodiorite to dacite porphyries, related to the Incaic magmatism (between 41 Ma and 30 Ma; Maksaev and Zentilli, 1999). At Gaby, basement rocks are represented by the Carboniferous Quebrada Escondida metavolcanic-sedimentary rocks and the Permian Pampa Elvira granodiorite complex. This basement is intruded by two Eocene porphyries, the dike-like Gaby and Crowded porphyries. In both deposits, a

well-developed supergene alteration profile is observed with a 120-500 m-thick supergene copper orebody at Zaldivar and a 250 m-thick copper oxide orebody at Gaby (Aguilar et al., 2003; Perelló et al., 2018). Both deposits lie beneath thick gravels pediment and comprises copper silicates as predominant Cu-bearing minerals, together with copper sulfates, copper phosphates and black-copper oxides.

The Gaoua porphyry Cu-Au district in southeastern Burkina Faso (Fig. 2C), is located within the West African craton (WAC) which consists of an Archean core, juxtaposed to Paleoproterozoic greenstone belts also known as the Boromo-Goren greenstone belt (Baratoux et al., 2011). The deposition of the Paleoproterozoic greenstone belt of the WAC took place during the Eburnean orogeny, around 2.25 to 2.15 Ga ago (Baratoux et al., 2011). These Boromo-Goren greenstone belt consists of volcanic to plutonic rocks affected by a greenschist facies regional metamorphism. These volcano-plutonic rocks were intruded by granitoids, emplaced from ca. 2250 Ma to 2060 Ma, and deformed successively by three deformation stages (Béziat et al., 2008; Baratoux et al., 2011; Baratoux et al., 2015). At a local scale, the Gaoua district is located at the southwestern margin of the Boromo Belt (Fig. 2C). The basement of the Gaoua porphyry copper deposit comprises a thick-sequence of mafic rocks (i.e. gabbro, basalt, andesite), followed by calc-akaline intrusive bodies (diorite, granodiorite, dolerite, granite, rhyolite). All the series underwent a regional greenschist-facies metamorphism (Baratoux et al., 2015). Hypogene copper mineralization is hosted by the greenschist facies volcanic flows and quartz-diorite intrusions (Le Mignot et al., 2017). This mineralization appears as veins, hydrothermal breccia filling or is disseminated within quartz-diorite porphyry stocks at Mont Biri, Diénémara, Gongondy and Bousséra (Fig. 2D; Le Mignot et al., 2017). The supergene copper ore of the Gaoua district is linked to the Tertiary history of the West African craton. During the Cenozoic, the onset of a hot and wet tropical climate, in alternation with dry seasons, in this tectonically stable craton and in addition to the low denudation rates in the region (2-20 m Ma^{-1}; Beauvais and Chardon, 2013) allowed for the formation of large and flat erosion surfaces a.k.a pediplains or regolith. These pediplains, which result from chemical and mechanical alteration of the bedrock (i.e. Birimian greenstone belts, Gunnell, 2003), sometimes overlie supergene mineralization of various economic importance, i.e. manganese at Tambao, and copper at Gaoua (Chardon et al., 2018). However, to the

best of our knowledge no studies have been published about the recognition and/or the characterization of the *in situ* SCM from the Gaoua porphyry Cu-Au district.

3. Analytical Procedures

Samples from five Cu-deposits in northern Chile and one Cu-Au deposit in Burkina Faso have been collected during a sampling campaigns in 2018 (i.e. Mina Sur, Damiana, El Cobre for exotic SCM) or were provided by mining geologists (i.e. Zaldivar, Gaby and Gaoua for *in situ* SCM). Mineralogical studies were carried out at the Géosciences Environnement Toulouse (GET, Université de Toulouse, France) using a polarizing microscope NIKON JLV 500 on polished thin sections. Backscattered electron images (BSE) as well as qualitative data were obtained using the JEOL JSM 6360 LV Scanning Electron Microscope (SEM) coupled to an energy dispersive spectrometry (EDS) analysis system at the GET laboratory. The analytical conditions used were 15kv for the acceleration voltage, 50 µm for the beam size while a tungsten filament was used as the electron source. Quantitative analyses as well as major element distribution maps were carried out at the Centre de Micro-Caractérisation Raimond Castaing (Université de Toulouse, France) using the CAMECA SXFive Electron Probe Micro-Analyzer (EPMA) on polished thin sections. The analytical conditions for the profiles were 2 µm for the beam size, 10 nA for the current intensity and an acceleration voltage of 15 keV. Data are reported in ESM 1. For the maps, the analytical settings were 100 nA for the current intensity, an acceleration voltage of 15 keV, a dwell time of 900 ms and a varying step size of 4 and 5 µm. Chemical studies, i.e. traces and REE elements analyses, were carried out at the GET laboratory using a Thermo-Fisher Element-XR, High Resolution Inductively Coupled Plasma Mass Spectrometry (HR-ICPMS) coupled to an ESI NWR213UC 213 nm laser ablation system (ns-LA). Tuning of the instrument as well as mass calibration were performed on NIST SRM 610 glass reference material, i.e. $^{238}U^{+}/^{232}Th^{+}$ between 0.95 and 1.05, oxide production < 0.5 % and a sensitivity > 20000 cps/ppm for ^{238}U. Laser ablation were carried out using a laser fluence of 3 J/cm^2, a repetition rate of 10 Hz and a 20 µm spot size. Ablated materials were transported in helium (450 mL/min) which was used as carrier gas. Each laser spot was ablated during 40s with 10s of background collection and 40s for the "wash-out". The isotopes monitored are ^{139}La, ^{140}Ce, ^{141}Pr, ^{146}Nd, ^{147}Sm, ^{151}Eu, ^{157}Gd, ^{159}Tb, ^{163}Dy, ^{165}Ho, ^{167}Er, ^{169}Tm, ^{173}Yb,

^{175}Lu. The internal and external calibration procedure suggested by Longerich et al. (1996) was used. The following standards were used: NIST SRM 610 reference glass as primary standard and 91500 zircon (as a proxy for the black chrysocolla and chrysocolla, see Wiedenbeck et al. 1995) as well as Durango apatite (as a proxy for pseudomalachite, see McDowell et al., 2005) as secondary, quality control standards (see Kahou et al., 2020). External measurement was carried out at the beginning and the end of each analytical session and each 15 spot analyses. Data reduction was carried out using the Iolite data reduction software (Paton et al., 2011). Operating conditions, traces and REE concentrations obtained on black chrysocolla, chrysocolla and pseudomalachite are reported in ESM 2.

4. Textural and chemical characterization of supergene copper mineralization

4.1 Textural features of SCM

To summarize the following description of the ore samples and the mineralogical assemblages, a synthetic paragenetic sequence is presented in Fig. 3.

4.1.1 The Mina Sur exotic SCM

The ore body at Mina Sur is ca. 2.2 km long, 1.2 km wide with a maximum thickness of about 110 m (Mortimer et al., 1977) and lies 2 Km south of the world-class Chuquicamata porphyry copper deposit. The copper mineralization is mainly composed of chrysocolla and atacamite that fill fractures in the bedrock as well as the porosity in the overlying sedimentary cover (Mortimer et al., 1977; Münchmeyer, 1996). Macroscopic scale observations of the samples selected for this study (Fig. 4A) show that the copper mineralization is mainly composed of chrysocolla either under the form of black Mn-rich angular millimeter size clasts (*a.k.a* black chrysocolla or copper pitch; see Throop and Buseck, 1971), or as millimetric turquoise to pale green Mn-poor bands coating both the black chrysocolla and the sedimentary clasts. Chrysocolla bands are intercalated with green micrometer size thin-bands of pseudomalachite. Atacamite, a copper chloride showing an acicular texture, is also present in small proportion. Under plane polarized light, black chrysocolla appears as black clasts, showing locally a concentric banding texture with black to brownish color variations (Fig. 4B). The chrysocolla bands (Fig. 4B) are made of microcrystalline aggregates with a strong birefringence in plane-polarized light

(Campos et al., 2015; Foote and Bradley, 1913; Menzies et al., 2015; Sun, 1963; Thompson, 1980). Pseudomalachite has an emerald-green to dark green color (Fig. 4B) and a low pleochroism in plane-polarized light (Berry, 1950; Shoemaker et al., 1977). Atacamite displays thin black prismatic crystal in cross-polarized light (Fig. 4C) and appears as overgrowths around the chrysocolla and pseudomalachite bands. Backscattered electron imaging (Fig. 4D) shows a more complex textural association between these minerals as chrysocolla and pseudomalachite display intergrowth textures. In some places, crystals of chrysocolla crosscut some pseudomalachite bands. Such textural relationships have been interpreted as resulting from dissolution-precipitation of pseudomalachite by chrysocolla (Crane et al., 2001). Finally, atacamite is present as prismatic crystals that grew on top of other mineral phases or also as filling available voids. Textural observations clearly shown that atacamite formed after chrysocolla and pseudomalachite.

4.1.2 The Damiana exotic SCM

At the scale of the outcrop, mineralization in both gravels (Fig. 5A) and bedrock fractures (Fig. 5B) appear as a homogeneous, cryptocrystalline blue-greenish mass. In hand specimens, chrysocolla is the most abundant copper mineral, followed, to a lesser extent, by copper wad, a term mainly used by miners to refer to a mixture of Mn, Fe, Cu oxyhydrates (Fam and Rojas, 1997; Menzies et al., 2015; Mote et al., 2001a; Pincheira et al., 2003).

In the ore found in the Damiana bedrock, optical microscopy observations confirm that chrysocolla predominates over copper wad and pseudomalachite. In the fractures, chrysocolla appears as greenish and heterogenous fillings. Sometimes, chrysocolla appears as micrometric concentric bands (Fig. 5C). Copper wad precedes chrysocolla and appears as thin coatings in fractures with a brown to dark brown color and a low pleochroism. Pseudomalachite was the last mineral to crystallize. It shows a thin coating texture under SEM, indistinguishable under the petrographic microscope and occurs as overgrowths on chrysocolla (Fig. 5D). Backscattered electron imaging shows a clear paragenetic sequence characterized by 1) copper wad showing colloform texture deposited as thin coatings within the bedrock fractures 2) massive chrysocolla is found within fractures in the bedrock usually on top of copper wad and 3) pseudomalachite filling the empty spaces left (Fig. 5D).

In the Damiana gravels, the SCM is deposited in the available empty spaces within the gravels (Fig. 5E). Chrysocolla is the dominant copper phase with lesser amounts of copper wad, pseudomalachite, microcrystalline quartz and apatite. Under plane polarized light, chrysocolla appears as millimetric greenish layers coating the gravels clasts. The texture is relatively homogeneous, with a low pleochroism and a strong relief (Fig. 5E). Pseudomalachite shows green to dark green color in plane polarized light, strong relief with a millimeter crystal size (Fig. 5E). Finally, quartz appears as euhedral micro-crystals, with low relief and birefringence (Fig. 5E). SEM-EDS analyses have shown a precipitation sequence characterized by chrysocolla precipitation coeval with colloform apatite, followed by the crystallization of pseudomalachite and microcrystalline quartz at a later stage (Fig. 5F). BSE images of chrysocolla displays either homogeneous texture or micrometer-scale banded texture, linked to variable Si/Cu ratios as shown by SEM-EDS analyses.

4.1.3 The El Cobre exotic SCM

At the scale of the outcrop, mineralization appears as massive cryptocrystalline light-blue to dark-blue masses filling the fractures. It may also be present as thin coating on the edge of some fractures (Fig. 6A, B). Chrysocolla is the most abundant Cu-bearing mineral, followed by minor copper wad and traces of pseudomalachite.

Under a petrographic microscope, a common paragenetic sequence is easily distinguishable for the filling of the fractures: first, copper wad is deposited as thin coatings covering the edges of the fractures, followed by the precipitation of chrysocolla (Fig. 6C). Finally, pseudomalachite and microcrystalline quartz are the last mineral phases to be deposited. At El Cobre, chrysocolla occurs mostly as cluster of concentric micrometer-scale laminae (Fig. 6C). Under SEM, chrysocolla shows a fairly homogeneous texture (Fig. 6D). Pseudomalachite crystallizes as concentric spherulitic and mammillary texture (as shown by SEM images, Fig. 6D) filling open spaces, impregnating bedrock fractures and overgrowing chrysocolla.

4.1.4 Zaldivar in situ SCM

The SCM at Zaldivar porphyry copper deposit extends over a thickness of about 500 m under the piedmont gravels (Monroy, 2000). At a macroscopic scale, the *in situ* SCM appears as emerald green to dark-green masses surrounding angular to sub-angular black clasts (Fig. 7A). The green to dark-green masses are made of brochantite and pseudomalachite while the black clasts are made of dark chrysocolla. Brochantite is the most abundant mineral phases whereas pseudomalachite and chrysocolla are less abundant. Under plane polarized light, both types of brochantite show a weak pleochroism (Fig. 7B). Prismatic-crystal shaped brochantite displays zoning characterized by a silica-rich core surrounded by druse crystal growth (Fig. 7B). Pseudomalachite occurs as light-green to green masses filling spaces similarly to brochantite (Fig. 7B). Chrysocolla is observed, under plane polarized light, as light- to dark-brown masses surrounding the clasts and filling the empty spaces or as coating the breccias (Fig. 7B). Chrysocolla displays a strong relief and shows a massive texture with syneresis cracks (Fig. 7C). SEM images clearly exhibit textural relationship between the copper-bearing minerals. Brochantite displays a markedly druse-crystal shape with micrometer-scale size (Fig. 7C) while pseudomalachite and brochantite show intergrowth textures (Fig. 7C). However, locally, brochantite seems to develop at the expense of a former assemblage of chrysocolla and pseudomalachite (Fig. 7C). Occasionally, pseudomalachite masses display homogeneous texture, without impurities. Copper wad forms micrometer-scale thin concentric bands coating pseudomalachite crystals (Fig. 7D).

4.1.5 Gaby Sur in situ SCM

In hand and core-logging samples, copper oxide mineralization appears either as veins (filling fractures) or disseminated within the porphyry (Fig. 8A). Chrysocolla is the most common mineral phases, followed by minor amounts of black copper oxides, brochantite and atacamite. Under the petrographic microscope, chrysocolla appears as light- to dark- green masses filling empty spaces (Fig. 8B). Under plane polarized light, chrysocolla shows a strong relief without cleavage. Chrysocolla presents no outward crystal form, although sometimes crystalline in internal structure (Fig. 8B). Copper wad is observed, under plane polarized light, as dark brown to black amorphous masses. Under SEM, chrysocolla displays a relative homogeneous texture with a lot of internal cracks and/or fractures (Fig. 8C). Copper wad is filling fractures and empty spaces and exhibits a colloform texture (Fig. 8C).

Brochantite clearly shows the direct replacement of sulfides (Fig. 8D) displaying impregnations and disseminations within the sulfides relicts and as coatings at the edges of the altered sulfides. Finally, atacamite coats both chrysocolla and brochantite as highlighted by SEM images (Fig. 8D).

4.1.6 Gaoua in situ SCM

SCM is disseminated inside the porphyries or fills some veins in association with primary sulfides. In hand samples, oxidized copper ore displays homogeneous light- to dark- blue masses filling veins (Fig. 9A). Under the petrographic microscope, these light to dark blue masses can be identified as chrysocolla, which is the most abundant oxidized Cu-bearing minerals (Fig. 9B). Under plane polarized light, chrysocolla appears as green to dark-green heterogeneous masses mainly found within fractures or as coating (Fig. 9B). Pseudomalachite and copper oxides (i.e. cuprite) are present in lesser amounts while no copper wad and atacamite have been found (Fig. 9C). Pseudomalachite is found as inclusions within the chrysocolla internal texture (Fig. 9D) while copper oxides exhibit a square granular shape due to corrosion and occurs as thin coatings as well as impregnating silica clasts as illustrated in Fig. 9D. Chrysocolla seems to replace cuprite and fills the empty spaces between the quartz crystals (Fig. 9D).

4.2 Chemical compositions of the main Cu-bearing minerals

4.2.1 Mineral chemistry

Quantitative major and minor element distributions of the studied SCM are reported in ESM 1.

In the exotic deposits (i.e. Mina Sur, Damiana or El Cobre), chrysocolla shows slightly variable proportion of CuO (~ between 50-55 wt. % at Mina Sur, 35-45 wt. % at Damiana and ~ 52 wt. % at El Cobre) and SiO_2 (values between ~ 40-50 wt. % at Mina Sur, 45-50 wt. % at Damiana and ~35-45 wt. % at El Cobre) as well as a variable proportion of H_2O (average between 0-10 wt. %). Al_2O_3, CaO, K_2O, MgO, FeO are also found as trace elements (Fig. 10A). Black chrysocolla (Fig. 10B), which is only found at Mina Sur, is distinguished from chrysocolla by a higher amount of MnO (up to 6 wt.%) and H_2O (10-20 wt.%) and a lower content in SiO_2 (20-40 wt.%) and CuO (~ 45-50 wt.%). Pseudomalachite displays more homogeneous composition with high CuO (~ 68.4 wt. % at Mina Sur,

between 63-70 wt. % at Damiana and ~ 67 wt. % at El Cobre) and P_2O_5 contents (average 24.2 wt. % at Mina Sur, 23-27 wt. % at Damiana and 27-28 wt. % at El Cobre) and low H_2O contents (5-10 wt. %) in all exotic deposits (Fig. 10C). Silica, aluminum, iron and calcium are also present as trace elements.

The compositional data obtained for the *in situ* SCM (i.e. Zaldivar, Gaby and Gaoua) are listed in ESM 1 and displayed in Fig. 10D for chrysocolla. At Zaldivar, the chemical composition of chrysocolla is consistent with previously published analyses (Newberg, 1967; Pinget, 2016) and display high SiO_2 (~ 43 wt. %) and CuO (~ 51 wt. %) contents with a low water content (~ 4 wt. %). Brochantite contains high proportion of Cu (CuO ~ 78 wt. % and 84 wt. %), and sulfate (SO_3 ~ 11-20 wt. %) while water was below the detection limits. Pseudomalachite shows CuO contents between 21-24 wt. %, P_2O_5 between 67-69 wt. % and H_2O contents between 5-8 wt. %. Chrysocolla is composed of CuO (~ 50 wt. %), SiO_2 (average between 39-47 wt. %) and variable water contents (average between 0-15 wt. %).

At Gaby, chrysocolla presents high CuO (~ between 45-58 wt. %) and SiO_2 contents (~ between 28-42 wt. %) and a varying proportion of H_2O (~ between 3-12 wt. %). Low concentrations of CaO (< 1 wt. %) is also found in chrysocolla. Brochantite, which replaces ancient sulfides, reveals high CuO (~ between 76 and 100 wt. %) and SO_3 (~ between 17-40 wt. %) contents. These wide range of values does not agree with the published values for brochantite (Mrose and Reichen, 1965) but rather highlights the ongoing replacement of sulfides relicts by brochantite and other Cu-phosphate minerals. EPMA-analyses carried out on atacamite show homogeneous Cl (~ 12-15 wt. %) and CuO concentrations (74-77 wt. %) and significant quantities of SiO_2 (up to 5 wt. %), emphasizing the presence of chrysocolla or silica impurities within the atacamite.

Finally, for the Gaoua deposit, EPMA analyses reveal that chrysocolla presents chemical compositions that are similar to those of the Atacama Desert. The SiO_2 and CuO contents vary from 35 wt. % to 48 wt. % (average ~ 41 wt. %) and from 41 wt. % to 51 wt. % (average ~ 46 wt. %) respectively while the Al_2O_3 contents can reach ~ 1.5 wt. %. In Gaoua, intra-layer compositional profiles of chrysocolla show a relatively homogeneous chemical composition with SiO_2 and CuO ranging from 35 wt. % to 45 wt. % and 43 wt. % to 51 wt. %, respectively. Low K_2O, CaO and Na_2O contents have also been detected. Pseudomalachite chemical analyses show high CuO (~ 67 wt. %) and P_2O_5 (~ 21 wt. %)

357 contents with minor amounts of SiO_2 (~ up to 2 wt. %). Aluminum, calcium and magnesium are present
358 as trace elements.

359 In order to better characterize the chemical homogeneity of the Cu-bearing minerals (i.e.
360 chrysocolla and pseudomalachite), distribution maps of Si, Cu and P were built for both type of deposits
361 (i.e. exotic and *in situ*). At Mina Sur, silica, copper and phosphorous show a fairly homogeneous
362 distribution in both minerals (Fig. 11A, B, C) although low-Cu and high-Si spots demonstrate the
363 presence of impurities and/or mineral inclusions. At Damiana and El Cobre, elemental distribution maps
364 show that the distribution of Si, Cu and P are rather homogenous in both chrysocolla and
365 pseudomalachite with the exception of the micro-cracks as seen in Fig. 12A-F. Nevertheless, a faint
366 concentric zoning can be observed in pseudomalachite at El Cobre (as shown in Fig. 12B, D, F), which
367 underlines concentric mineral layering and reveals the crosscutting relationship between chrysocolla
368 and pseudomalachite. For chrysocolla and pseudomalachite from Zaldivar, elemental distribution maps
369 are homogeneous for P, Si and Cu and show a faint zoning for Si, Cu and P in the copper wad (Fig.
370 13A, C, E). Finally, for the Gaby deposit, distribution maps for Si and Cu at the boundaries between
371 chrysocolla and copper wad, show growth bands within the copper wad contrasting with the
372 homogenous distributions within the chrysocolla (Fig. 13B, D).

373 *4.2.2 Rare earth elements*

374 Results are presented in ESM 2 for REE and in Fig. 14. Except for Damiana and El Cobre, all
375 the chrysocolla and pseudomalachite samples have REE concentrations above the detection limits.

376 REE data of chrysocolla from exotic (Fig. 14A) and *in situ* (Fig. 14B) SCM have been plotted in
377 a chondrite-normalized spider diagram (McDonough and Sun, 1995). Most of the chrysocolla from both
378 exotic and *in situ* deposits, show a flat pattern for all the REE with a slightly depleted spectrum for
379 HREE, a strong negative Ce-anomaly and a small negative Eu-anomaly. Chrysocolla from the *in situ*
380 SCM of Zaldivar appears as an outlier, with notably lower REE contents and a strong positive Ce-
381 anomaly. Chrysocolla from Gaby and Gaoua has REE contents that are ten times higher than those from
382 Zaldivar, with a strong negative Ce-anomaly. REE contents of chrysocolla from Mina Sur are ten times
383 lower than any other exotic deposits without a markedly negative Ce-anomaly. Chrysocolla from

Damiana displays LREE contents ten times higher than those from Mina Sur and El Cobre. Black chrysocolla from Mina Sur show a strong negative Ce-anomaly, a flat HREE spectrum with HREE contents that are ten times higher than chrysocolla from the same deposit.

With the exception of Damiana, the REE patterns for pseudomalachite found in the exotic and *in situ* SCM show high LREE and HREE concentrations when compared to REE contents of chrysocolla and black chrysocolla (Fig. 14C, D). The REE spectrum at El Cobre shows concentrations up to ten times higher than those obtained at Damiana and Mina Sur, especially for LREE. For Mina Sur and El Cobre, LREE spectrum show a strong negative Ce-anomaly while LREE data at Damiana show an almost flat spectrum without any noticeable negative Ce-anomaly. In spite of their distinct, negative Ce-anomaly, REE contents from El Cobre are more Ce-rich that those from Damiana and Mina Sur. Compared to the LREE spectrum, the HREE spectrum from Mina Sur and Damiana shows a slight enrichment while at El Cobre, the HREE displays a slight depleted spectrum (Fig. 4C). The notable exception is the pseudomalachite REE pattern from the Zaldivar deposit (Fig. 14D), which shows a HREE depleted spectra compared to LREE and a weak negative Eu-anomaly. We also note that the LREE contents in pseudomalachite from Zaldivar are systematically an order of magnitude higher than pseudomalachite from Mina Sur and Damiana.

5. Discussion

5.1 Physicochemical controls for the SCM formation

In all the studied *in situ* and exotic SCM, chrysocolla is by far the most abundant copper-bearing mineral and predominates over copper wad, atacamite and pseudomalachite.

In the *in situ* SCM deposits, the mineral parageneses are almost similar with minor copper wad at Zaldivar and Gaby, which precedes abundant chrysocolla in the three deposits, followed by lesser amount of pseudomalachite at Zaldivar. At Gaoua, cuprite is the main second stage mineral followed by pseudomalachite. This paragenetic sequence suggests that all these deposits have undergone the similar processes of *in situ* supergene oxidation. In detail, at Zaldivar and Gaby, textural and mineralogical features show that copper sulfides were replaced by oxidized sulfate-Cu minerals (Fig. 7C and Fig. 8C). The oxidation process is accompanied by a lower pH (Anderson, 1982) and a loss of

copper (i.e. by downward or lateral migration) as shown by the lower copper contents in sulfate minerals compared to supergene sulfides. The main thermodynamic constraints for abundant chrysocolla precipitation are pH and $H_4SiO_4^0$ (aq) activity (Crane et al., 2001; Yates et al., 1998). Chrysocolla precipitates when the pH exceed ~ 5 (Yates et al., 1998). Precipitation of chrysocolla is thus commonly explained by changing conditions from acid (pH < 5) to neutral or low-alkaline (pH < 9) due to the neutralization of the acidic copper solutions during fluid-rock interaction (Newberg, 1967). It also means that most of the minerals that contributes to lowers the pH (i.e. pyrite and chalcopyrite) are leached or do not have the capacity to increase the pH. As suggested by Crane et al. (2001), when $H_4SiO_4^0$ (aq) is the dominant species in the copper solution, chrysocolla will precipitate at a pH ~ 7. Inversely, when $H_2PO_4^-$ (aq) is the dominant species in the copper solutions, pseudomalachite will precipitate. This can explain the precipitation of pseudomalachite at Zaldivar and Gaoua. Generally, cuprite crystallizes as replacement of the primary sulfides (Schwartz, 1934) and is rapidly oxidized to hydrate the copper phases. In Fig. 9D, chrysocolla seems to replace cuprite which confirms the assumption of Schwartz (1934).

In the exotic SCM (i.e. Mina Sur, Damiana, El Cobre), the same paragenetic sequence is clearly observed: small amount of copper wad, followed by abundant precipitation of chrysocolla and pseudomalachite. At Mina Sur atacamite appears as overgrowths on chrysocolla. At Damiana, apatite growth is coeval to the first phase of chrysocolla. At Damiana and El Cobre, pseudomalachite and microcrystalline quartz are linked to the second crystallization stage event. Except for Mina Sur characterized by the presence of reworked angular clasts of black chrysocolla linked to mechanical transportation or *in situ* breaking, all three deposits show mineral textures resulting from the deposition of copper transported in solution from a source (i.e. porphyry copper deposits) to a sink (i.e. the adjacent basins). This requires a progressive neutralization of the mineralizing fluids originating from the upstream oxidizing ore from porphyry copper deposits (Münchmeyer, 1996; Sillitoe, 2005). According to Newberg (1967) and Fernández-Mort et al. (2018), chrysocolla can precipitate as soon as the pH reaches value between ~ 5 and 9 with an optimum value of ~7. Chrysocolla is formed by the interaction between a copper-rich fluid and SiO_2 (Yates et al., 1998). Copper comes from the porphyry while SiO_2

438 can come from either the porphyry host rocks or from the gravels present in the basins (e.g. altered
439 feldspars). Finally, the good porosity and permeability of the host gravels will favor the precipitation
440 of chrysocolla.

441 The paragenetic relationship between chrysocolla and pseudomalachite records pH variation.
442 Figure 7 from Crane et al. (2001) and Figure 10 from Fernández-Mort et al. (2018) have shown that a
443 slight variation of the pH in copper-rich solutions can lead to the saturation of either chrysocolla or
444 pseudomalachite together with the $H_4SiO_4^0$ (aq) activity. This could explain the alternation of
445 chrysocolla and pseudomalachite observed at Mina Sur and the presence of second stage
446 pseudomalachite at Damiana and El Cobre. The fact that, in both *in situ* or exotic SCM, pseudomalachite
447 has been found as thin bands or as thin coatings around chrysocolla, implies that the chemistry of
448 copper-rich solutions from the parental porphyry is not constant but has changed according to the pH
449 variation and the $H_4SiO_4^0$ (aq) and $H_2PO_4^-$ (aq) ions activity.

450 At Damiana and El Cobre, the last mineral to precipitate was the microcrystalline quartz. Bustillo
451 (2010) has shown that microcrystalline quartz is stable at pH < 9 whereas at pH > 9, calcite is broadly
452 stable. At pH between 5 and 9, chrysocolla and pseudomalachite tend to co-precipitate. When the
453 mineralizing fluids is depleted in copper, microcrystalline quartz can precipitate (Dold, 2006). The
454 meaning of microcrystalline quartz precipitation can be discussed in terms of a silicification process
455 (Bustillo, 2010), favored by the silica content, temperature, host-rock permeability and pH. Highly
456 silica oversaturated solutions will lead to poorly-ordered silica phases (e.g. opal and amorphous silica)
457 while slightly saturated solutions conduct to more ordinated forms (i.e. quartz and chalcedony). This
458 transition may reflect a dilution of the silicification process as shown by Thiry et al. (2006) and
459 highlighted by Fernández-Mort et al. (2018) at Tesoro Central exotic copper deposit. Indeed, the
460 transition from chrysocolla to microcrystalline quartz, observed in our samples, could be a proof of a
461 silicification process.

462 The fact that no copper carbonates were observed in both type of deposits could be explained by
463 either the combination of high $H_4SiO_4^0$ (aq) activity and a pH maximum value of ~ 9 for the copper-
464 rich solutions or by the fact that the fluid was too depleted in copper after chrysocolla and
465 pseudomalachite formation to promote copper carbonates precipitation.

Ultimately, when the climate become more arid (or hyperarid), atacamite, a copper salt highly soluble in fresh water, started to crystallize. This is well exemplified by the atacamite needles overgrowing pseudomalachite at Mina Sur (Fig.5D) linked to salt-rich water circulation in the hyperarid conditions of the Atacama Desert (Reich et al., 2008). The fact that atacamite was not found at Gaoua can be explained either by the absence of saline fluids which could have promoted the formation of atacamite or salt minerals (e.g. gypsum, anhydrite), or by their late destabilization in the context of modern semi-arid climatic conditions (the West African Craton never experienced a hyperarid climate; Séranne, 1999).

As observed in most of the deposits, chrysocolla and copper wad show concentric banding texture which suggests chemical variations of the mineralizing fluids as already mentioned by Nelson et al. (2007) and Campos et al. (2015). The banding textures observed within chrysocolla have also been explained by Nelson et al. (2007) as the result of biogenic processes, suggesting bacterial involvement in the formation of *in situ* (i.e. at Gaby) and exotic (i.e. at Mina Sur, Damiana and El Cobre) SCM.

5.2 REE concentration in supergene copper minerals

Beside the presence of oxidized copper rich minerals such as silicates, phosphates and sulfates, the existence of oxidizing conditions in the studied localities is supported by the geochemical characterization of the supergene copper minerals (chrysocolla and pseudomalachite) where REE spectra (Fig. 14) are characterized by Ce-anomalies. As shown by Goldschmidt (1937) and Braun et al. (1990), Ce is the only LREE to present two oxidation states (Ce^{3+} and Ce^{4+}) in a low-T environment. This makes Ce highly sensitive to redox processes. In fact, the oxidation state of Ce is mainly controlled by the pH. At low pH, water could reduce Ce^{4+} to Ce^{3+} whereas if the pH value increases, Ce^{3+} is oxidized to Ce^{4+} (Bouchaud et al., 2012). Bouchaud et al. (2012) have also shown, by experimental studies, that Ce^{3+} and Ce^{4+} are soluble in meteoric water at neutral to alkaline pH values. Additionally, Estrade et al. (2019 and references therein), have shown that the precipitation of Ce, either as Ce^{4+} or Ce^{3+}, within supergene environments, is linked to the depth of the supergene column. In the upper part of the column, within more oxidizing and higher pH, Ce^{4+} precipitates in Ce-rich minerals such as cerianite (CeO_2) or associated with Mn- and Fe- oxyhydroxydes. Consequently, the supergene copper

minerals will display negative Ce-anomaly due to the Ce^{4+} consumption by cerianite or Mn-Fe oxyhydroxydes. This is the case for chrysocolla and pseudomalachite presented in this study who recorded negative Ce-anomaly, except for chrysocolla from Zaldivar. Conversely, in the lower part of the supergene column, under low pH and reduced conditions, Ce^{3+} predominates over Ce^{4+} and no Ce-rich minerals such as cerianite or Mn-Fe oxyhydroxydes can precipitate. Therefore, Ce will be available in the environment and captured by Cu-rich supergene minerals that will consequently display positive Ce-anomaly as seen for example for chrysocolla at Zaldivar. Similarly, Decrée et al. (2015) have shown that REE spectrum in heterogenite (a supergene cobalt mineral, CoOOH) can display negative Ce-anomaly when this mineral co-precipitates with Mn- and Fe-oxides in the upper part of the oxidation profile and positive Ce-anomaly when heterogenite forms in the deeper part of the oxidation profile. The negative Ce-anomalies in exotic copper deposits will further support continuous oxidizing conditions. By contrast, the REE patterns from *in situ* supergene copper minerals (i.e. chrysocolla and pseudomalachite), which show both positive and negative Ce-anomalies, might reflect changes in the redox conditions during the leaching process, above the porphyry, both in time (reducing to oxidizing conditions) and space, i.e. from oxidizing conditions at the top (with Ce^{4+} predominates) toward reducing conditions at depth (with Ce^{3+} predominates).

If we focus on the REE concentration processes for both *in situ* and exotic deposits, the REE distribution within chrysocolla and pseudomalachite are heterogenous. Pseudomalachite from El Cobre and Zaldivar contains ten times more REE than those from the other deposits. Furthermore, REE patterns of chrysocolla are contrasted, as the REE contents in Damiana are ten times higher compared to those from Mina Sur, while the REE contents of Zaldivar are ten times lower than those from Gaby and Gaoua. Indeed, in supergene environments, the REE-bearing minerals control the budget and the distribution of the REE. The weathering of the primary REE-bearing minerals (i.e. zircon, monazite and xenotime) will induce either the redistribution of the REE within the newly formed supergene copper minerals (e.g. chrysocolla and pseudomalachite) or the consumption of the REE by secondary REE-bearing minerals (i.e. allanite, bastnesite, rhabdophane; Braun et al., 2018). For instance, the absence of secondary REE-bearing minerals at El Cobre and Zaldivar could explain the high REE concentrations found in pseudomalachite from both deposits whereas possible precipitation of apatite and rhabdophane

(i.e. two secondary phosphate REE-bearing minerals) in the other deposits (i.e. at Mina Sur and Damiana) could explain the low REE contents in pseudomalachite. Similarly, the low REE content in chrysocolla at Mina Sur and Zaldivar (Fig. 14A, B) could be explained by the precipitation of secondary REE-bearing silicates minerals (e.g. allanite, bastnesite) that trapped the REE.

5.3 Necessary conditions for the genesis and preservation of oxidized SCM

In the Atacama Desert of northern Chile and in southwestern Burkina Faso, tectonics (i.e. Incaic orogeny in Northern Chili and Eburnean orogeny in Burkina Faso) and climatic (i.e. semi-arid to arid climate) settings were combined to favor supergene alteration of porphyries and the formation of thick *in situ* supergene copper orebodies (Sillitoe, 2005; Sillitoe and McKee, 1996) and/or exotic-Cu deposits (Fernández-Mort et al., 2018, 2018; Hartley and Rice, 2005; Münchmeyer, 1996; Riquelme et al., 2017; Sillitoe, 2005). To produce an oxidized supergene copper mineralization, three conditions are necessary. First, tectonic uplift will bring the primary porphyry stock and hypogene sulfides close to the earth surface where oxidizing conditions, controlled by the level of water table, prevail. Second, under favorable climatic conditions, the oxidation of sulfides will produce acidic solutions which will transport copper down and laterally, in the subjacent area, to form an oxidized copper ores when copper solution reach saturation (Fernández-Mort et al., 2018; Reich and Vasconcelos, 2015). Finally, once the supergene column is formed, favorable climatic conditions as well as moderate erosion rate can favor SCM preservation. The fact that, although both areas have experienced different tectonic styles, the supergene copper minerals from northern Chile and SW Burkina Faso are identical and share the same chemical compositions implies that they both underwent similar climatic evolutions, i.e. from semi-arid to arid, during the mineralization processes. However, if Northern Chile has evolved towards a hyperarid climate for the past ~10 m.y., responsible for the formation of atacamite, the SW Burkina Faso area has only experienced a semi-arid climate since the Eocene (Monsels, 2016). According to Hartley and Rice (2005), who published a compilation of supergene copper deposits ages in the Atacama Desert, the formation of *in situ* SCM took place between 36 Ma and 6 Ma. More recently, Riquelme et al., (2017) and Kahou et al., (2020) have published ages between ca. 25-12 Ma and ca. 19 Ma for the formation of the Centinela and Mina Sur exotic copper deposits respectively, i.e. ages that

548 are within the range found for the *in situ* SCM. As stated by Sillitoe (2005) and Sanchez et al. (2018),
549 in Chile, the processes necessary for the formation of well-developed oxidized SCM profile can take
550 anything from a million to ten millions of years and ceased at the onset of hyperaridity. In SW Burkina
551 Faso, the age of the SCM deposit is unknown but the phases responsible for the exhumation of the
552 porphyry towards oxidizing conditions were contemporanous with lateritization/bauxitisation
553 processes, i.e. between 59 Ma and 3 Ma (Beauvais and Chardon, 2013; Gunnell, 2003). These
554 exhumation phases were controlled by evolving weathering conditions and took place at rates lower
555 than 20 m/m.y. (Beauvais and Chardon, 2013). The comparison between Chilean and African SCM
556 suggest that the preservation of the supergene deposits is due to a favorable combination of slow erosion
557 rates and aridity.

558 Another necessary factor for the genesis of oxidized SCM can be related to evaporation process.
559 In the southern part of the Atacama Desert, a stable isotope study by Bissig and Riquelme (2010) has
560 shown that meteoric waters were affected by high evaporation rates to favor the deposition of supergene
561 alunite. In the same manner, Fernández-Mort et al. (2018) also highlighted that evapoconcentration was
562 the main parameter to form the exotic SCM of Tesoro Central. Although no isotope studies have been
563 carried out in this study, this evaporation process can be involved in the formation of both *in situ* and
564 exotic SCM deposits from Chile but also in the *in situ* SCM from Burkina Faso.

565 5.4 Oxidized SCM characterization: key for an exploration success

566 Oxidized SCM are the result of supergene alteration of hypogene sulfides, namely pyrite and
567 chalcopyrite from any sulfide-rich deposit. This supergene alteration produces a vertical zonation
568 consisting on a Fe- and Al-rich leached cap depleted in Cu, followed by an oxidized horizon moderately
569 enriched in copper (up to 1 wt. % of Cu) and at the bottom a secondary sulfide enrichment zone, highly
570 enriched in copper (up to 2 wt. % of Cu) formed below the paleo water table (Chávez, 2000; Sillitoe,
571 2005). As stated by Chavez (2000), the distribution of oxidized copper minerals can be used as
572 exploration keys. For example, as shown by our study, the broad distribution of chrysocolla within *in*
573 *situ* SCM are interpreted as characteristic of a geochemically mature supergene system and the
574 formation of a well-developed *in situ* oxidized SCM. In fact, both types of oxidized SCM represent an

575 important target for numerous exploration and mining companies as their exploitation is
576 environmentally friendly compare to process required for the recovery of copper from sulfide ore. As a
577 result, mineralogical characterization of SCM can provides some useful keys to better improve the
578 metallurgical treatment.

579 To date, mapping exploration program combined with geophysical and geochemical studies,
580 successfully located oxidized and enriched porphyry copper deposits buried beneath piedmonts gravels.
581 Moreover, geomorphological and sedimentological studies are powerful tools to discover new *in situ*
582 and exotic SCM. As proposed by Riquelme et al. (2017), the exploration of these deposits, buried under
583 gravels and ignimbrite, needs to take into consideration both the landscape evolution and the
584 depositional history of the piedmont gravels. The study of the landscape and the piedmont evolution
585 has also been presented as a major guide for the exploration of supergene ore by Chardon et al. (2018)
586 in Burkina Faso. When the conditions are favorable, supergene alteration of porphyry copper deposit
587 also leads to the deposition of exotic SCM, hosted within piedmont gravels or underlying bedrock
588 fractures. The presence of exotic copper deposits is indicative of the existence of primary copper
589 porphyry deposits somewhere upstream and can be used as exploration tool. Although in some cases,
590 the source of these deposits are known (e.g. Chuquicamata porphyry for Mina Sur and Salvador
591 porphyry for Damiana, see Munchmeyer, 1996), the sources of some exotic-Cu deposits remain
592 unknown (e.g. Tesoro and Lagarto exotic-Cu deposits; Munchmeyer, 1996; Sillitoe, 2005). Therefore,
593 the mineralogical and geochemical characterization of the supergene copper minerals should be
594 implemented during exploration strategies. For instance, the predominance of chrysocolla over copper
595 wad in an exotic-Cu deposit is indicative of a lateral migration of copper-rich solutions within a radius
596 of 2 to 6 km around the primary porphyry copper deposit. When combined with mass-balance
597 calculation model and geomorphology, mineralogical studies can assess the geochemical maturity of
598 the oxidized ore of the porphyry copper deposit and the directions followed by the copper solutions
599 from the primary copper deposits to the sink (Alpers and Brimhall, 1989; Mote et al., 2001b).
600 Consequently, an integrated study involving geomorphology, sedimentology and geochronological
601 together with a mineralogical and geochemical characterization of the oxidized SCM must be taken into
602 account for enhanced exploration success.

6. Conclusions

Supergene copper mineralization from three exotic and two *in situ* Cu-deposits from the Atacama Desert in Northern Chile and the Gaoua *in situ* Cu-Au district in Burkina Faso have been studied in details. Mineralogical and chemical characterization of these SCM provide new insights on the genesis of these deposits. Chrysocolla, which precipitates after copper wad, is the main Cu-bearing minerals and shows similar textures and chemical compositions in both *in situ* and exotic SCM. Precipitation of chrysocolla reflects the progressive evolution of the mineralizing fluids from acidic (pH < 5) to neutral or low-alkaline (pH < 9) conditions during fluid-rock interaction. Chrysocolla is then followed by the crystallization of pseudomalachite in exotic deposits due to changes of both pH and H_2PO_4 activity of the Cu-bearings fluids (i.e.). Geochemical analyses emphasize the strong oxidizing conditions required for the formation of oxidized SCM and show that REE distribution and Ce-anomaly are linked to the pH evolution, the depth of the supergene column and the presence of primary and secondary REE-bearing minerals. The fact that almost the same mineralogy and geochemical patterns are observed on six different deposits, on different location and geodynamic context, point out the fact that the processes involve in the formation of these deposits are very similar, i.e. progressive neutralization of the acidic copper solutions that lead to chrysocolla precipitation at neutral pH, high $H_2PO_4^-$ (aq) activity together with low $H_4SiO_4^0$ (aq) activity that permit pseudomalachite formation, and silicification process that lead to the late crystallization of microcrystalline quartz.

The role of regional and local controls on the formation and preservation of supergene mineralization is now well-understood and requires a subtle balance between tectonics, climate and geomorphology. The formation of such deposits requires several steps with first the exhumation and weathering of the primary porphyry deposit to ensure surface oxidizing processes and a preservation favored by an environment characterized by moderate erosion and rain fall to prevent mechanical abrasion and leaching of the newly formed deposits and finally, a possible key role played by evaporation processes. This equilibrium has been achieved in both Northern Chile and SW Burkina Faso where similar mineralization processes have been involved to form SCM.

Acknowledgments: We would like to thank the geologists from CODELCO-Chile for providing access to the Mina Sur and Damiana open-pit mines. We also want to thank geologists from the Zaldivar and Gaby copper mines for giving us samples. We thank Didier Béziat, Athanase Naré, Naba Séta and Pascal Ouiya who helped us to have access to samples from the Gaoua Cu-Au district. Special thanks to Fabienne de Parseval, Thierry Aigouy, Sophie Gouy, Aurélie Marquet and François-Xavier d'Abzac who helped during thin sections preparation, SEM, EPMA and LA-ICP-MS analyses.

This work was supported by the program funding of the Institut Carnot ISIFoR and the TelluS Program of CNRS/INSU. We acknowledge the LMI Copedim, an IRD research program, the Université Paul Sabatier (Toulouse, France) as well as Universidad Católica del Norte (Antofagasta, Chile). Finally, we want to gratefully acknowledge the Society of Economic Geologists Foundation for the Hugh McKinstry fund (SRG 20-15) received by Zia Steven Kahou.

References

Aguilar, A., Gomez, M., Pérez, P., 2003. Discovery and Geology of the Undeveloped Codelco's Gaby Copper Deposit. Presented at the Congreso Geologico Chileno, Concepcion, p. 1.

Alpers, C.N., Brimhall, G.H., 1989. Paleohydrologic evolution and geochemical dynamics of cumulative supergene metal enrichment at La Escondida, Atacama Desert, northern Chile. Economic Geology 84, 229–255. https://doi.org/10.2113/gsecongeo.84.2.229

Alpers, C.N., Brimhall, G.H., 1988. Middle Miocene climatic change in the Atacama Desert, northern Chile: Evidence from supergene mineralization at La Escondida. Geological Society of America Bulletin 100, 1640–1656. https://doi.org/10.1130/0016-7606(1988)100<1640:MMCCIT>2.3.CO;2

Amilibia, A., Sàbat, F., McClay, K.R., Muñoz, J.A., Roca, E., Chong, G., 2008. The role of inherited tectono-sedimentary architecture in the development of the central Andean mountain belt: Insights from the Cordillera de Domeyko. Journal of Structural Geology 30, 1520–1539. https://doi.org/10.1016/j.jsg.2008.08.005

Anderson, J., 1982. Characteristics of leached capping and techniques of appraisal, in: Advandces in Geology of the Porphyry Copper Deposits, Southwestern North America. University of Arizona Press, Tucson, pp. 275–296.

Baratoux, L., Metelka, V., Naba, S., Jessell, M.W., Grégoire, M., Ganne, J., 2011. Juvenile Paleoproterozoic crust evolution during the Eburnean orogeny (~2.2–2.0Ga), western Burkina Faso. Precambrian Research 191, 18–45. https://doi.org/10.1016/j.precamres.2011.08.010

Baratoux, L., Metelka, V., Naba, S., Ouiya, P., Siebenaller, L., Jessell, M.W., Naré, A., Salvi, S., Béziat, D., Franceschi, G., 2015. Tectonic evolution of the Gaoua region, Burkina Faso: Implications for mineralization. Journal of African Earth Sciences 112, 419–439. https://doi.org/10.1016/j.jafrearsci.2015.10.004

Beauvais, A., Chardon, D., 2013. Modes, tempo, and spatial variability of Cenozoic cratonic denudation: The West African example: Cenozoic cratonic denudation. Geochemistry, Geophysics, Geosystems 14, 1590–1608. https://doi.org/10.1002/ggge.20093

Berry, L.G., 1950. On pseudomalachite and Cornetite. American Mineralogist 35, 365–385.

Béziat, D., Dubois, M., Debat, P., Nikiéma, S., Salvi, S., Tollon, F., 2008. Gold metallogeny in the Birimian craton of Burkina Faso (West Africa). Journal of African Earth Sciences 50, 215–233. https://doi.org/10.1016/j.jafrearsci.2007.09.017

Bissig, T., Riquelme, R., 2010. Andean uplift and climate evolution in the southern Atacama Desert deduced from geomorphology and supergene alunite-group minerals. Earth and Planetary Science Letters 299, 447–457. https://doi.org/10.1016/j.epsl.2010.09.028

Bissig, T., Riquelme, R., 2009. Contrasting Landscape Evolution and Development of Supergene Enrichment in the El Salvador Porphyry Cu and Potrerillos-El Hueso Cu-Au Districts, Northern Chile. Society of Economic Geologists Special Publication 14, 59–68.

Bouchaud, B., Balmain, J., Bonnet, G., Pedraza, F., 2012. pH-distribution of cerium species in aqueous systems. Journal of Rare Earths 30, 559–562. https://doi.org/10.1016/S1002-0721(12)60091-X

Bouzari, F., Clark, A.H., 2002. Anatomy, Evolution, and Metallogenic Significance of the Supergene Orebody of the Cerro Colorado Porphyry Copper Deposit, I Región, Northern Chile. Economic Geology 97, 1701–1740.

Braun, J.-J., Pagel, M., Muller, J.-P., Bilong, P., Michard, A., Guillet, B., 1990. Cerium anomalies in lateritic profiles. Geochimica et Cosmochimica Acta 54, 781–795.

Braun, J.-J., Riotte, J., Battacharya, S., Violette, A., Oliva, P., Prunier, J., Maréchal, J.-C., Ruiz, L., Audry, S., Subramanian, S., 2018. REY-Th-U Dynamics in the Critical Zone: Combined Influence of Reactive Bedrock Accessory Minerals, Authigenic Phases, and Hydrological Sorting (Mule Hole Watershed, South India). Geochemistry, Geophysics, Geosystems 19, 1611–1635. https://doi.org/10.1029/2018GC007453

Bustillo, M.A., 2010. Silicification of Continental Carbonates, in: Developments in Sedimentology. Elsevier, Oxford, pp. 153–174. https://doi.org/10.1016/S0070-4571(09)06203-7

Campos, E., Menzies, A., Sola, S., Hernandez, V., Riquelme, R., Barraza, M., 2015. Understanding Exotic-Cu Mineralisation: Part I - Characterisation of Chrysocolla, in: 3:1153. Presented at the 13th SGA Biennal meeting, 13th SGA Biennal meeting, Nancy, France.

Chardon, D., Grimaud, J.-L., Beauvais, A., Bamba, O., 2018. West African lateritic pediments: Landform-regolith evolution processes and mineral exploration pitfalls. Earth-Science Reviews 179, 124–146. https://doi.org/10.1016/j.earscirev.2018.02.009

Chávez, W.X., 2000. Supergene Oxidation of Copper Deposits: Zoning and Distribution of Copper Oxide Minerals. SEG Newsletter, Society of Economic Geologists 41, 13.

Cornejo, P., Tosdal, R.M., Mpodozis, C., Tomlinson, A.J., Rivera, O., Fanning, C.M., 1997. El Salvador, Chile Porphyry Copper Deposit Revisited: Geologic and Geochronologic Framework. International Geology Review 39, 22–54. https://doi.org/10.1080/00206819709465258

Crane, M.J., Sharpe, J.L., Williams, P.A., 2001. Formation of chrysocolla and secondary copper phosphates in the highly weathered supergene zones of some Australian deposits. Records of the Australian Museum 53, 49–56. https://doi.org/10.3853/j.0067-1975.53.2001.1323

Cuadra, P., Rojas, G., 2001. Oxide mineralization at the radomiro tomic porphyry copper deposit. Economic Geology 96, 387–400.

Decrée, S., Pourret, O., Baele, J.-M., 2015. Rare earth element fractionation in heterogenite (CoOOH): implication for cobalt oxidized ore in the Katanga Copperbelt (Democratic Republic of Congo). Journal of Geochemical Exploration 159, 290–301. https://doi.org/10.1016/j.gexplo.2015.10.005

Dilles, J.H., Tomlinson, A.J., García, M., Alcota, H., 2011. The geology of the Fortuna Granodiorite Complex, Chuquicamata district, Northern Chile: relation to porphyry copper deposits. Presented at the SGA Biennial Meeting 11th, SGA Biennial Meeting 11th, Antofagasta, Chile, pp. 399–401.

Dold, B., 2006. Geochemical modeling of the exotic mineralization of the Exotica deposit at Chuquicamata, Chile, in: XI Congreso Geologico Chileno. Presented at the XI Congreso Geologico Chileno, Antofagasta, Chile, p. 4.

Estrade, G., Marquis, E., Smith, M., Goodenough, K., Nason, P., 2019. REE concentration processes in ion adsorption deposits: Evidence from the Ambohimirahavavy alkaline complex in Madagascar. Ore Geology Reviews 112, 103027. https://doi.org/10.1016/j.oregeorev.2019.103027

Fam, R., Rojas, O., 1997. Eventos de mineralizacion Exotica de Cu en el distrito de Chuquicamata, II region Chile. Presented at the Congreso Geologico Chileno VIII, Congreso Geologico Chileno VIII, Antofagasta, Chile, pp. 1923–1927.

Fernández-Mort, A., Riquelme, R., Alonso-Zarza, A.M., Campos, E., Bissig, T., Mpodozis, C., Carretier, S., Herrera, C., Tapia, M., Pizarro, H., Muñoz, S., 2018. A genetic model based on evapoconcentration for sediment-hosted exotic-Cu mineralization in arid environments: the case of the El Tesoro Central copper deposit, Atacama Desert, Chile. Mineralium Deposita 53, 775–795. https://doi.org/10.1007/s00126-017-0780-2

Foote, H.W., Bradley, W.M., 1913. On solid solutions in Minerals. IV. The composition of amorphous minerals as illustrated by chrysocolla. American Journal of Science 36, 180–184.

Garreaud, R.D., Molina, A., Farias, M., 2010. Andean uplift, ocean cooling and Atacama hyperaridity: A climate modeling perspective. Earth and Planetary Science Letters 292, 39–50. https://doi.org/10.1016/j.epsl.2010.01.017

Goldschmidt, V.M., 1937. The principles of distribution of chemical elements in minerals and rocks. The seventh Hugo Müller Lecture, delivered before the Chemical Society on March 17th, 1937. J. Chem. Soc. 0, 655–673. https://doi.org/10.1039/JR9370000655

Gunnell, Y., 2003. Radiometric ages of laterites and constraints on long-term denudation rates in West Africa. Geology 31, 131. https://doi.org/10.1130/0091-7613(2003)031<0131:RAOLAC>2.0.CO;2

Gustafson, L.B., Hunt, J.P., 1975. The porphyry copper deposit at El Salvador, Chile. Economic Geology 70, 857–912. https://doi.org/10.2113/gsecongeo.70.5.857

Gustafson, L.B., Orquera, W., Mcwilliams, M., Castro, M., Olivares, O., Rojas, G., Maluenda, J., Mendez, M., 2001. Multiple Centers of Mineralization in the Indio Muerto District, El Salvador, Chile. Economic Geology 96, 2.

Hartley, A.J., Rice, C.M., 2005. Controls on supergene enrichment of porphyry copper deposits in the Central Andes: A review and discussion. Mineralium Deposita 40, 515–525. https://doi.org/10.1007/s00126-005-0017-7

Kahou, Z.S., Brichau, S., Poujol, M., Duchêne, S., Campos, E., Leisen, M., d'Abzac, F.-X., Riquelme, R., Carretier, S., 2020. First U-Pb LA-ICP-MS in situ dating of supergene copper mineralization: case study in the Chuquicamata mining district, Atacama Desert, Chile. Mineralium Deposita. https://doi.org/10.1007/s00126-020-00960-2

Le Mignot, E., Siebenaller, L., Béziat, D., André-Mayer, A.-S., Reisberg, L., Salvi, S., Velasquez, G., Zimmermann, C., Naré, A., Franceschi, G., 2017. The Paleoproterozoic Copper-Gold Deposits of the Gaoua District, Burkina Faso: Superposition of Orogenic Gold on a Porphyry Copper Occurrence? Economic Geology 112, 99–122. https://doi.org/10.2113/econgeo.112.1.99

Longerich, H.P., Jackson, S.E., Gunther, D., 1996. Laser ablation inductively coupled plasma mass spectrometric transient signal data acquisition and analyte concentration calculation. Journal of Analytical Atomic Spectrometry 11, 899–904.

Maksaev, V., Zentilli, M., 1999. Fission Track Thermochronology of the Domeyko Cordillera, Northern Chile: Implications for Andean Tectonics and Porphyry Copper Metallogenesis. Exploration and Mining Geology 8, 65–89.

Marsh, T.M., Einaudi, M.T., McWilliams, M., 1997. 40Ar/39Ar Geochronology of Cu-Au and Au-Ag Mineralization in the Potrerillos District, Chile. Economic Geology 92, 784–806.

May, G., Hartley, A.J., Chong, G., Stuart, F., Turner, P., Kape, S.J., 2010. Eocene to Pleistocene lithostratigraphy, chronostratigraphy and tectono-sedimentary evolution of the Calama Basin, northern Chile. Andean Geology 32, 33–58. https://doi.org/10.5027/andgeoV32n1-a04

May, G., Hartley, A.J., Stuart, F.M., Chong, G., 1999. Tectonic signatures in arid continental basins: an example from the Upper Miocene–Pleistocene, Calama Basin, Andean forearc, northern Chile. Palaeogeography, Palaeoclimatology, Palaeoecology 151, 55–77. https://doi.org/10.1016/S0031-0182(99)00016-4

McDonough, W.F., Sun, S. -s., 1995. The composition of the Earth. Chemical Geology 120, 223–253. https://doi.org/10.1016/0009-2541(94)00140-4

McDowell, F.W., McIntosh, W.C., Farley, K.A., 2005. A precise 40Ar–39Ar reference age for the Durango apatite (U–Th)/He and fission-track dating standard. Chemical Geology 214, 249–263. https://doi.org/10.1016/j.chemgeo.2004.10.002

Menzies, A., Campos, E., Hernandez, V., Sola, S., Riquelme, R., 2015. Understanding Exotic-Cu Mineralisation: Part II - Characterisation of Black Copper ("Cobre Negro"). Presented at the 13th SGA Biennial Meeting, 13th SGA Biennial Meeting, Nancy, France.

Monroy, C., 2000. Nueves antecedentes geologicos del porfido cuprifero Zaldivar II Region, Chile. Presented at the Congreso Geologico Chileno, 9th, Actas, Puerto Varas, pp. 293–297.

Monsels, D.A., 2016. Bauxite deposits in Suriname: Geological context and resource development. Netherlands Journal of Geosciences - Geologie en Mijnbouw 95, 405–418. https://doi.org/10.1017/njg.2015.28

Mortimer, C., Munchmeyer, C., Urqueta, I., 1977. Emplacement of the Exotica orebody, Chile. Institute of Mining and Metallurgy Transactions 86, B121–B127.

Mote, T.I., Becker, T.A., Renne, P., 2001a. Chronology of Exotic Mineralization at El Salvador, Chile, by 40Ar/39Ar Dating of Copper Wad and Supergene Alunite. Economic Geology 96, 351–366.

Mote, T.I., Brimhall, G.H., Tidy-Finch, E., Muller, G., Carrasco, P., 2001b. Application of mass-balance modeling of sources, pathways, and sinks of supergene enrichment to exploration, discovery of the Quebrada Turquesa exotic copper orebody, El Salvador District, Chile. Economic Geology 96, 367–386.

Mpodozis, C., Cornejo, P., 2012. Cenozoic Tectonics and Porphyry Copper Systems of the Chilean Andes. Society of Economic Geologists Special publication 16, 32.

Mpodozis, C., Ramos, V., 1989. The Andes of Chile and Argentina. Geology of the Andes and its Relation to Hydrocarbon and Mineral Resources 59–90.

Mrose, M.E., Reichen, L.E., 1965. Evidence for the identity of Kamarezite with Brochantite, Cu4(SO4)(OH)6. The American Mineralogist 50, 1450–1457.

Münchmeyer, C., 1996. Exotic deposits - products of lateral migration of supergene solutions from porphyry copper deposits. Andean copper deposits : new discoveries, mineralization, styles and metallogeny 43–58.

Nelson, M., Kyser, K., Clark, A., Oates, C., 2007. Carbon Isotope Evidence for Microbial Involvement in Exotic Copper Silicate Mineralization, Huinquintipa and Mina Sur, Northern Chile. Economic Geology 102, 1311–1320. https://doi.org/10.2113/gsecongeo.102.7.1311

Newberg, D.W., 1967. Geochemical implications of chrysocolla-bearing alluvial gravels. Economic Geology 62, 932–956. https://doi.org/10.2113/gsecongeo.62.7.932

Ossandón, G., Fréraut, R., Gustafson, L.B., Lindsay, D.D., Zentilli, M., 2001. Geology of the Chuquicamata Mine : A Progress Report. Economic Geology 96, 249–270.

Paton, C., Hellstrom, J., Paul, B., Woodhead, J., Hergt, J., 2011. Iolite: Freeware for the visualisation and processing of mass spectrometric data. Journal of Analytical Atomic Spectrometry 26, 2508. https://doi.org/10.1039/c1ja10172b

Perelló, J., González, A., Monroy, C., 2018. Geologic Controls on Hypogene Mineralization at the Zaldívar Porphyry Copper-Gold-Molybdenum Deposit, Escondida District, Northern Chile. Society of Economic Geologists 21, 271–292. https://doi.org/10.5382/SP.21.12

Pincheira, M., Kelm, U., Helle, S., Dagnino, A., Osses, M., 2003. Las fases de cobre negro en yacimientos exoticos: nuevos antecedentes mineralógicos, texturales y composicionales. Minerales 58, 13–18.

Pinget, M.-C., 2016. Supergene enrichment and exotic mineralization at Chuquicamata, Chile. (Unpublished PhD thesis). Université de Genève, Suisse.

Ransome, F.L., 1912. Copper deposits near Superior, Arizona. U.S. Geological Survey Bulletin 540-D, 139–158.

Reich, M., Palacios, C., Parada, M.A., Fehn, U., Cameron, E.M., Leybourne, M.I., Zúñiga, A., 2008. Atacamite formation by deep saline waters in copper deposits from the Atacama Desert, Chile: evidence from fluid inclusions, groundwater geochemistry, TEM, and 36Cl data. Mineralium Deposita 43, 663–675. https://doi.org/10.1007/s00126-008-0184-4

Reich, M., Vasconcelos, P.M., 2015. Geological and Economic Significance of Supergene Metal Deposits. Elements 11, 305–310. https://doi.org/10.2113/gselements.11.5.305

Riquelme, R., Tapia, M., Campos, E., Mpodozis, C., Carretier, S., González, R., Muñoz, S., Fernández-Mort, A., Sanchez, C., Marquardt, C., 2017. Supergene and exotic Cu mineralization occur during periods of landscape stability in the Centinela Mining District, Atacama Desert. Basin Research 1, 31. https://doi.org/10.1111/bre.12258

Rivera, S., Alcota, H., Proffett, J., Diaz, J., Leiva, G., Vergara, M., 2012. Update of the Geologic Setting and Cu–Mo Deposits of the Chuquicamata District, Northern Chile. In: Harris M, Camus F (eds) Geology and Genesis of major copper deposits and districts of the world: a tribute to Richard H. Sillitoe and J.W. Hedenquist. Society of Economic Geologists Special publication, 19–54.

Rojas, R., Muller, G., 1994. “Damiana”: Uno de los yacimientos tipo" Exoticos" de El Salvador. Presented at the Congreso Geologico Chileno, 7th, Actas, Concepcion, pp. 892–896.

Sanchez, C., Brichau, S., Riquelme, R., Carretier, S., Bissig, T., Lopez, C., Mpodozis, C., Campos, E., Regard, V., Hérail, G., Marquardt, C., 2018. Exhumation history and timing of supergene copper mineralisation in an arid climate: New thermochronological data from the Centinela District, Atacama, Chile. Terra Nova 30, 78–85. https://doi.org/10.1111/ter.12311

Scheuber, E., Bogdanic, T., Jensen, A., Reutter, K.-J., 1994. Tectonic Development of the North Chilean Andes in Relation to Plate Convergence and Magmatism Since the Jurassic, in: Reutter, Klaus-Joachim, Scheuber, E., Wigger, P.J. (Eds.), Tectonics of the Southern Central Andes. Springer Berlin Heidelberg, Berlin, Heidelberg, pp. 121–139. https://doi.org/10.1007/978-3-642-77353-2_9

Scheuber, E., Reutter, K.-J., 1992. Magmatic arc tectonics in the Central Andes between 21° and 25°S. Tectonophysics, Andean geodynamics 205, 127–140. https://doi.org/10.1016/0040-1951(92)90422-3

Schwartz, G.M., 1934. Paragenesis of the oxidized ores of copper. Economic Geology 29, 55–75. https://doi.org/10.2113/gsecongeo.29.1.55

Séranne, M., 1999. Early Oligocene stratigraphic turnover on west Africa continental margin: a signature of the Tertiary greenhouse to icehouse transition? Terra Nova 11, 135–140.

Shoemaker, G.L., Anderson, J.B., Kostiner, E., 1977. Refinement of the crystal structure of pseudomalachite. American Mineralogist 62, 1042–1048.

Sillitoe, R.H., 2010. Porphyry Copper Systems. Economic Geology 105, 3–41. https://doi.org/10.2113/gsecongeo.105.1.3

Sillitoe, R.H., 2005. Supergene Oxidized and Enriched Porphyry Copper and Related Deposits. Society of Economic Geologists 100th anniversary volume, 723–768.

Sillitoe, R.H., McKee, E.H., 1996. Age of supergene oxidation and enrichment in the Chilean porphyry copper province. Economic Geology 91, 164–179. https://doi.org/10.2113/gsecongeo.91.1.164

Sillitoe, R.H., Mortimer, C., Clark, A.H., 1968. A chronology of landform evolution and supergene mineral alteration, southern Atacama Desert, Chile. Institute of Mining and Metallurgy Transactions 77, B166–B169.

Sillitoe, R.H., Perelló, J., 2005. Andean Copper Province: Tectonomagmatic Settings, Deposit Types, Metallogeny, Exploration, and Discovery. Society of Economic Geologists 100th, 845–890.

Sun, M.-S., 1963. the nature of chrysocolla from inspiration mine. The American Mineralogist 48, 649–658.

Thiry, M., Milnes, A.R., Rayot, V., Simon-CoinÇon, R., 2006. Interpretation of palaeoweathering features and successive silicifications in the Tertiary regolith of inland Australia. Journal of the Geological Society 163, 723–736. https://doi.org/10.1144/0014-764905-020

Thompson, W.A., 1980. Chrysocolla pseudomorphs from Ray, Arizona. Mineralogical Record 11, 248–250.

Throop, A.H., Buseck, P.R., 1971. Nature and Origin of Black Chrysocolla at the Inspiration Mine, Arizona. Economic Geology 66, 1168–1175. https://doi.org/10.2113/gsecongeo.66.8.1168

Tomlinson, A.J., Blanco, N., Maksaev, V., Dilles, J.H., Grunder, A.L., Ladino, M., 2001. Geologia de la Precordillera Andina de Quebrada Blanca - Chuquicamata, Regiones I y II (20°30’ 22°30’ S). SERNAGEOMIN 2, 444.

Urzua, F., 2009. Geology, geochronology, and structural evolution of La Escondida copper district, northern Chile: (Unpublished PhD thesis). University of Tasmania.

Wiedenbeck, M., Allé, P., Corfu, F., Griffin, W.L., Meier, M., Oberli, F., Quadt, A.V., Roddick, J.C., Spiegel, W., 1995. Three Natural Zircon Standards for U-Th-Pb, Lu-Hf, Trace Element and Ree Analyses. Geostandards Newsletter 19, 1–23. https://doi.org/10.1111/j.1751-908X.1995.tb00147.x

Yates, D.M., Joyce, K.J., Heaney, P.J., 1998. Complexation of copper with polymeric silica in aqueous solution. Applied Geochemistry 13, 235–241.

Captions

Fig. 1 Schematic representation of the relationships between hypogene porphyry copper mineralization and supergene copper mineralization (SCM) forming *in situ* and exotic copper deposits (modified after Sillitoe, 2005)

Fig. 2 Location and geological map of the studied areas. a) location of major SCM in the world map, including Atacama Desert of northern Chile and Gaoua Cu-Au district (after Sillitoe, 2010). b) Structural map of the Precordillera of northern Chile (after Mpodozis and Cornejo, 2012) showing the location of the *in situ* and exotic SCM deposit studied. Black squares mark the location of the Chuquicamata, Salvador and Potrerillos mining districts in which the Mina Sur, Damiana and El Cobre exotic SCM deposits are located, respectively c) Location (black square) of the Gaoua Cu-Au district within the simplified geological map of Burkina Faso (BGB: Boromo Greenstone Belt; HGB: Houndé Greenstone Belt after Béziat et al., 2008). d) Detailed geological map of the Gaoua Cu-Au district showing the location of the Mont Biri, Diénémara, Gongondy and Bousséra *in situ* supergene Cu-Au occurrences (Baratoux et al., 2015; Le Mignot et al., 2017)

Fig. 3 Synthetic paragenetic sequence for the studied exotic and *in situ* SCM deposits. Stage 1 corresponds to the main supergene oxidation while Stage 2 corresponds to the late filling empty spaces

Fig. 4 Sample and thin sections photographs showing the relationships between Mina Sur copper minerals. a) Black chrysocolla (B-Ccl) is coated by chrysocolla (Ccl) and pseudomalachite (Psm) bands. b) Plane-polarized light photograph showing black chrysocolla clast (B-Ccl) coated by chrysocolla (Ccl) and pseudomalachite (Psm) bands. c) Cross-polarized light and d) SEM photomicrographs showing black chrysocolla clast (B-Ccl) coated by chrysocolla (Ccl) laminae and pseudomalachite (Psm) bands and an overgrowth of atacamite needles (Ata) on chrysocolla and pseudomalachite

Fig. 5 Sample and thin sections photographs showing the relationships between Damiana copper minerals. Chrysocolla (Ccl) filling empty spaces and porosity of the gravels at a) Damiana gravels and fractures at b) Damiana bedrock. c) Cross-polarized light photograph showing chrysocolla (Ccl) and copper wad (Cwad) filling fractures at Damiana bedrock. d) SEM photomicrographs showing copper wad (Cwad) banding mammillary texture and chrysocolla (Ccl), and pseudomalachite (Psm) coating chrysocolla. e) Plane-polarized light photograph of chrysocolla (Ccl) filling porosity of the gravels at

Damiana gravels and pseudomalachite and microcrystalline quartz filling empty spaces. f) SEM photomicrographs showing chrysocolla (Ccl) coeval with apatite (Apa) filling porosity of the gravels and pseudomalachite (Psm) crystallizing in empty spaces

Fig. 6 Sample and thin sections photographs showing the relationships between El Cobre copper minerals. a, b) Chrysocolla (Ccl) filling fractures of the altered andesite bedrock. c) Plane-polarized light photograph showing copper wad (Cwad), chrysocolla (Ccl) and pseudomalachite filling fractures of the andesite bedrock. d) SEM photomicrograph showing chrysocolla (Ccl)coating on copper wad (Cwad) banding mammillary texture and chrysocolla (Ccl) and pseudomalachite (Psm) and amorphous quartz filling empty spaces

Fig. 7 Sample and thin sections photographs showing the relationships between Zaldivar copper minerals. a) Hand-samples of Zaldivar supergene copper minerals. b) Plane-polarized light photograph showing relicts of altered sulfides replaced by brochantite and brown chrysocolla and pseudomalachite gradually replacing brochantite. c, d) SEM photomicrographs showing a complex textural relationship between brochantite, copper wad (Cwad) thin band, chrysocolla and pseudomalachite

Fig. 8 Sample and thin sections photographs showing the relationships between Gaby copper minerals. a) Hand-samples of Gaby showing chrysocolla (Ccl) filling fractures in the Gaby micro-diorite host-rock. b) Plane-polarized light photograph showing copper wad (Cwad) and chrysocolla filling fractures of the host-rock. c, d) SEM photomicrographs showing c) copper wad thin band and fractured and homogeneous texture of chrysocolla, crystallizing within host-rock veins and d) an altered sulfide replaced by brochantite and chrysocolla, and atacamite (Ata) overgrowing on brochantite

Fig. 9 Sample and thin sections photographs showing the relationships between Gaoua copper minerals. a) Hand-samples of Gaoua showing chrysocolla (Ccl) filling fractures in the Gaoua quartz-andesite host-rock. b) Plane-polarized light photograph showing chrysocolla (Ccl) filling fractures of the host-rock. c) Plane-polarized light and d) SEM photographs showing thin green crystals of cuprite (Cup) and pseudomalachite (Psm) coating on quartz crystals and chrysocolla filling empty spaces and corrodes cuprite

Fig. 10 Representative diagrams of oxidized supergene copper mineralization chemical analyses showing in Triplot diagrams. a) chrysocolla chemical analyses from Mina Sur, Damiana and El Cobre

exotic SCM deposits. b) black chrysocolla chemical analyses from Mina Sur exotic SCM deposit. c) Pseudomalachite chemical analyses from Mina Sur, Damiana and El Cobre exotic SCM deposits. d) Chrysocolla chemical analyses from Zaldivar, Gaby and Gaoua *in situ* SCM deposits

Fig. 11 EPMA chemical characterization of supergene copper minerals from Mina Sur exotic SCM deposit. a) Si map b) Cu map and c) P map at the transition between black chrysocolla (B-Ccl), chrysocolla (Ccl) and pseudomalachite (Psm) to highlight the homogeneity/heterogeneity distribution of silicon, copper and phosphorus. Dotted square represents the area analyzed

Fig. 12 EPMA chemical characterization of supergene copper minerals from a, c, e) Damiana and b, d, f) El Cobre exotic SCM deposits. a, b) Si map c, d) Cu map and e, f) P map at the transition between chrysocolla (Ccl) and pseudomalachite (Psm) to highlight the distribution of silicon, copper and phosphorus within these minerals. Dotted square represents the area analyzed

Fig. 13 EPMA chemical characterization of supergene copper minerals from Zaldivar and Gaby *in situ* SCM deposit. a, b) Si c, d) Cu and e) P maps at the transition between chrysocolla (Ccl), copper wad (Cwad) and pseudomalachite (Psm) to highlight the distribution of silicon, copper and phosphorus within these minerals. Dotted square represents the area analyzed

Fig. 14 Chondrite normalized REE patterns for oxidized supergene copper minerals. a, b) REE patterns of chrysocolla and black chrysocolla from exotic and *in situ* SCM deposits. c, d) REE patterns of pseudomalachite from exotic and *in situ* SCM deposits. Chondrite normalizing values are taken from McDonough and Sun (1995)

ESM 1 Summary of supergene copper minerals EPMA analyses from exotic and *in situ* SCM deposits

ESM 2 Summary of LA-ICP-MS analyses carried out on supergene copper minerals from exotic and *in situ* SCM deposits. Operating conditions and data obtained on standards are also listed

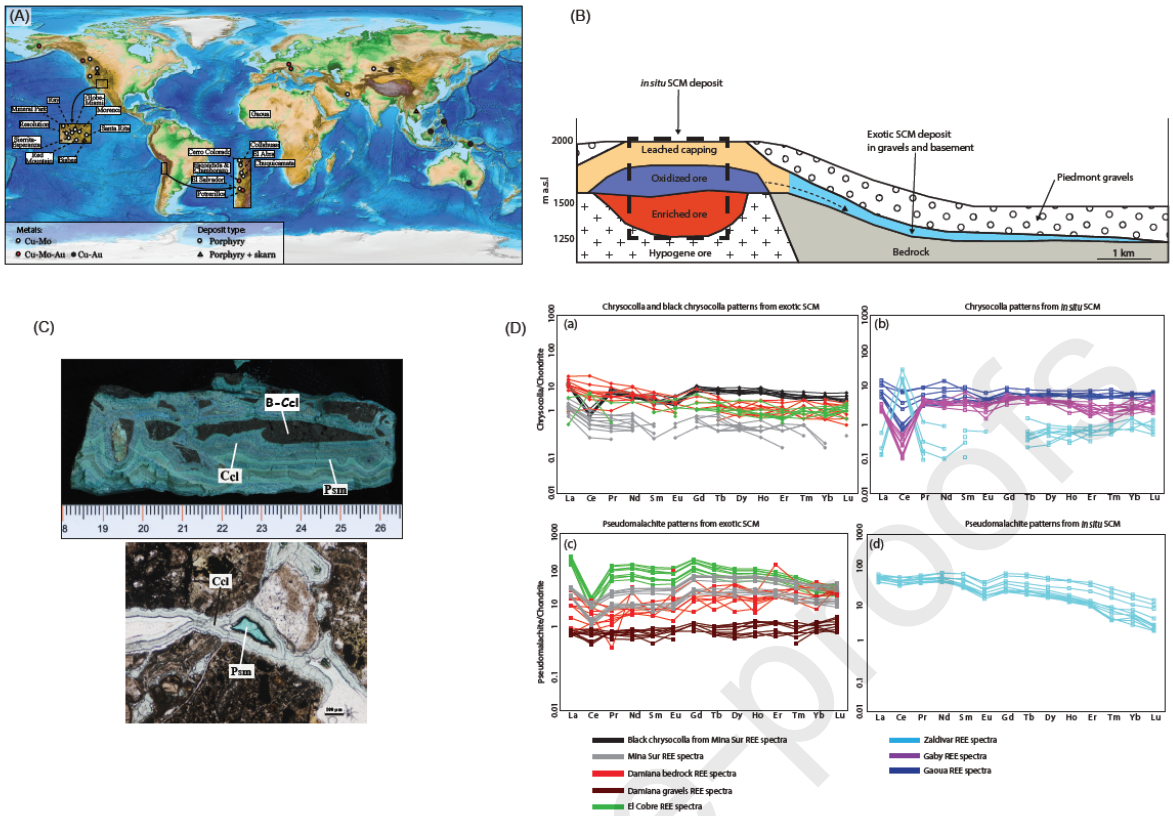

Highlights

- Supergene copper mineralization (SCM) from Atacama Desert and SW of Burkina Faso
- Paragenesis and chemical characterization of SCM from different geodynamic context
- The same mineralogy and geochemical patterns are observed in both areas
- REE study suggests oxidizing conditions to form supergene copper mineralization
- Geological and climatic controls involve in the genesis of these SCM are similar